

Dual Strategy of Molecular-Weight Control and Ionic Doping in Poly(benzodifurandione) for Energy-Efficient Neuromorphic OECTs

José Carlos Pérez Martínez,¹ Ignacio Sanjuán*,¹ David Franco,¹ Isaac Sánchez-Márquez,¹ Baurzhan Ilyassov,² Qun-Gao Chen,³ Wen-Ya Lee,³ Chu-Chen Chueh,⁴ and Antonio Guerrero*¹

¹ Institute of Advanced Materials (INAM), Universitat Jaume I, 12006 Castelló, Spain.

² Astana IT University, Mangilik El avenue 55/11, Business center EXPO, block C1, Astana, 010000, Kazakhstan

³ Department of Chemical Engineering and Biotechnology, National Taipei University of Technology, Taipei 106344, Taiwan

⁴ Department of Chemical Engineering, National Taiwan University, Taipei 10617, Taiwan

Corresponding authors: I. Sanjuán (i.sanjuan@uji.es), A. Guerrero (aguerrer@uji.es)

Abstract

Poly(benzodifurandione) (PBFDO) has emerged as a promising n-type mixed conductor for organic electrochemical transistors (OECTs), combining outstanding electrical properties with long-term stability. However, its intrinsically high electrical conductivity, advantageous for bioelectronics, leads to excessive operating currents and elevated energy demands in neuromorphic computing. To overcome this limitation, we introduce two complementary strategies that decouple intrinsic conductivity from computing performance. First, molecular-weight engineering via benzofuranone end-capping yields a reduced-chain-length polymer (PBFDO-BF) with substantially suppressed intrinsic conductivity. Second, ionic doping with 5 wt.% LiTFSI enhances ion-mediated conductance modulation in PBFDO-BF, enabling pronounced synaptic functionality. The combined PBFDO-BF + LiTFSI system achieves optimal OECT operation, characterized by enhanced modulation, pronounced hysteresis, and spike-dependent plasticity with long-term potentiation/depression (LTP/LTD), while reducing operating currents by approximately one order of magnitude compared to pristine PBFDO. In MNIST-based convolutional neural-network (CNN) simulations, this device delivers superior performance, attaining 97.78% training accuracy, 98.57% inference accuracy, and the lowest cumulative energy consumption to reach $\approx 90\%$ accuracy. These findings establish molecular-weight control coupled with ionic doping as an effective design paradigm to optimize PBFDO for energy-efficient neuromorphic OECTs, without compromising stability or solution processability.

Introduction

The development of high-performance n-type conducting polymers remains one of the foremost challenges in organic electronics. Compared to the p-type counterparts, n-type polymers have historically suffered from limited air stability, lower electron mobility, and susceptibility to oxidative degradation,¹ resulting in a scarcity of stable, solution-processable candidates and a bottleneck in advancing organic electronic technologies.

In this context, the emergence of poly(benzodifurandione)(PBFDO) represents a transformative breakthrough in this field, combining exceptional thermal, ambient, and electrochemical stability with remarkable solution processability, characteristics that position it as a leading candidate for next-generation organic electronic applications. Recent reports of PBFDO achieving ultrahigh n-type conductivities have catalyzed intense research interest across multiple disciplines.^{2,3} The exceptional electrical properties and solution processability of PBFDO polymer have enabled the integration into a diverse array of organic electronic devices, demonstrating versatility across multiple applications, such as organic thermoelectric, organic photovoltaic, optoelectronic devices, and organic electrochemical transistors (OECTs).⁴⁻¹³

OECTs are particularly attractive for neuromorphic computing due to their operational analogy to biological synapses.¹³⁻¹⁵ In biological memory systems, electrical impulses travel along neuronal axons and are communicated to neighboring neurons through synaptic junctions. This process relies on the release and uptake of neurotransmitters, enabling signal transmission with remarkable energy efficiency. In contrast, OECTs function by incorporating organic materials as a conductive channel between source and drain electrodes. In this case, channel conductivity is modulated through reversible volumetric doping and de-doping processes. The insertion or extraction of ions within the organic layer leads to changes in channel conductance.^{13,16}

Authors have reported a PBFDO polymer that enables exceptionally high electrical conductivity (>2000 S/cm). However, when this polymer is integrated into OECTs, its exceptionally high conductivity results in extremely large device currents, undermining low-power operation essential for neuromorphic applications.¹⁷ To further adapt PBFDO polymer for neuromorphic computing, it is vital to modulate its conductivity while retaining the inherent stability to oxygen and moisture. Recent studies indicate that the polymer's chain length or molecular weight can strongly influence its electronic and optical properties.¹⁸

In addition, recent works have demonstrated that mobile ions can strongly influence the electronic properties of PBFDO polymer. In particular, proton migration within the polymer matrix has been shown to modulate local doping states, induce spatially resolved conductivity changes, and enable neuromorphic functionalities in OECT configurations.¹³ These findings highlight that, despite its intrinsically electronic nature, PBFDO is highly sensitive to its ionic environment, suggesting that ion-polymer interactions may provide a powerful handle to tune its charge transport behavior. Moreover, doping with ionic salts such as lithium bis(trifluoromethanesulfonyl)imide (LiTFSI) is known to affect the polymer

microstructure, preferentially penetrating amorphous regions and promoting mixed ionic/electronic conduction.¹⁹ Ohayon et al. demonstrated that adding organic salts such as LiTFSI as additives to n-type OMIEC precursor solutions enables the fabrication of OECTs with increased transconductance and stability. The salt-added as-deposited films showed improved backbone planarity, a distinct porous morphology, and lower water uptake, which must be the cause of the enhanced performance.²⁰

In this work, we investigate two different strategies to tune the PBFDO conductivity for low-power neuromorphic devices. The first involves modifying the polymer chain length to adjust its molecular weight, and the second includes the incorporation of LiTFSI to optimize ion injection and promote efficient mixed ionic/electronic conduction. The performance of the OECTs is validated through simulated neural networks for image recognition and an analysis of the energy consumption. Our results provide new insight into ion–electron conduction in intrinsically doped conjugated polymers and offer design principles for tuning hybrid ionic–electronic transport in next-generation organic electronic materials.

Results and Discussion

Two polymers with different molecular weights and doping levels have been synthesized as described in the Experimental Section. In this work, we define PBFDO as a high-conductivity polymer with a high molecular weight, synthesised using previously reported methods.²¹ PBFDO is synthesized with the monomer benzodifurandione (H-BFDO), which contains two 5-member-ring cyclic lactones that are polymerizable. Since both lactones are equivalent, the elongation of the PBFDO could continue technically endlessly until solubility limits are reached, which results in long polymer chains. In addition, another polymer is synthesized in this work by adding benzofuranone (BF) to the reaction mixture (H-BFDO in DMSO) with the aim of reducing the molecular weight and conductivity of the as-prepared polymer. BF only contains one cyclic lactone end group, limiting the polymerization to one side and thus acting as an end-capping agent. The as-prepared PBFDO-derived polymer, thereafter referred to as PBFDO-BF, is expected to have shorter chains (**Figure 1**). The synthesis of both polymers is confirmed by ¹H-RMN (**Figure SI1a**). The confirmation is indirect through the conversion of H-BFDO and BF (disappearance of the signals), as neither polymer nor BF signals are observed in the ¹H-RMN. The lack of ¹H-NMR resonances can be attributed to its conjugated backbone and paramagnetic signal broadening arising from the doping. The electrical conductivity of both polymers was measured using the 4-probe method and the voltammetry technique (**Figure SI1b and c**). The electrical conductivity obtained for the PBFDO and PBFDO-BF is 47.38 and 0.38 S cm⁻¹, respectively. The two orders of magnitude lower conductivity of PBFDO-BF agrees with a decrease in the polymer chain length and reduced doping. We performed rheological measurements, which revealed that the PBFDO solution in DMSO displayed a markedly higher viscosity than PBFDO-BF in all the shear-rate range used (**Figure SI2e**), suggesting that PBFDO exhibits stronger effective intermolecular interactions among

chains and/or higher network formation. The viscosity is also in agreement with a decreased length in the polymer chain for the PBFDO-BF. Moreover, dynamic light scattering (DLS) (**Figure SI2a-d**) measurements revealed clear differences in the organization of the two polymers in DMSO solution. PBFDO showed a narrow size distribution centered at a few nanometers, whereas PBFDO-BF exhibited a bimodal distribution, with a main population in the 100 nm range of hydrodynamic radius and a second contribution extending into the 800 nm range, indicating the formation of larger aggregates in solution. We hypothesize that the longer chains of PBFDO, with higher doping as well, interact more strongly by coulombic attraction, hydrogen bonds, and π - π stacking between the aromatic chains leading to a smaller hydrodynamic radius.

Next, we fabricated the OECTs by depositing both PBFDO and PBFDO-BF thin films onto glass substrates with patterned ITO interdigitated electrodes, as described in the Experimental Section. We prepared OECTs with PBFDO and PBFDO-BF, and the same polymers with LiTFSI at 5 wt.% (~20 nm measured by profilometry), and we measured their current-voltage response and the UV-vis-NIR spectra. The current-voltage (I - V) responses without electrolyte (**Figure 1b**) confirm that the PBFDO is significantly more conductive than the PBFDO-BF, in agreement with the 4-probe measurements. The addition of LiTFSI to the films gives rise to a slight increase in currents for the PBFDO and a more noticeable raise in current for the PBFDO-BF. The UV-vis-NIR spectra (**Figure 1c**) show that PBFDO is considerably more doped than PBFDO-BF, exhibiting a five-fold higher intensity in the 900–2000 nm polaron–bipolaron band associated with doping. Despite its markedly higher doping level, PBFDO also displays a stronger absorption at 490 nm, assigned to the π - π^* transition of the neutral aromatic polymer chains, as well as a higher intensity in the 550–850 nm region, where both polaron-related absorption and intermolecular charge transfer in the neutral polymer contribute. These results prove that PBFDO possesses longer polymer chains. Upon addition of LiTFSI to PBFDO, the intensity of the 485 nm band and the 550–850 nm region decreases, while the 900–2000 nm polaron–bipolaron band increases, confirming the doping effect of LiTFSI. However, this effect is relatively limited, as PBFDO is already highly doped. In contrast, the addition of LiTFSI to PBFDO-BF leads to a more relatively pronounced increase in doping, with the intensity of the polaron–bipolaron band nearly doubling. However, the doping level of the latter is still noticeably lower than that of PBFDO + LiTFSI 5%.

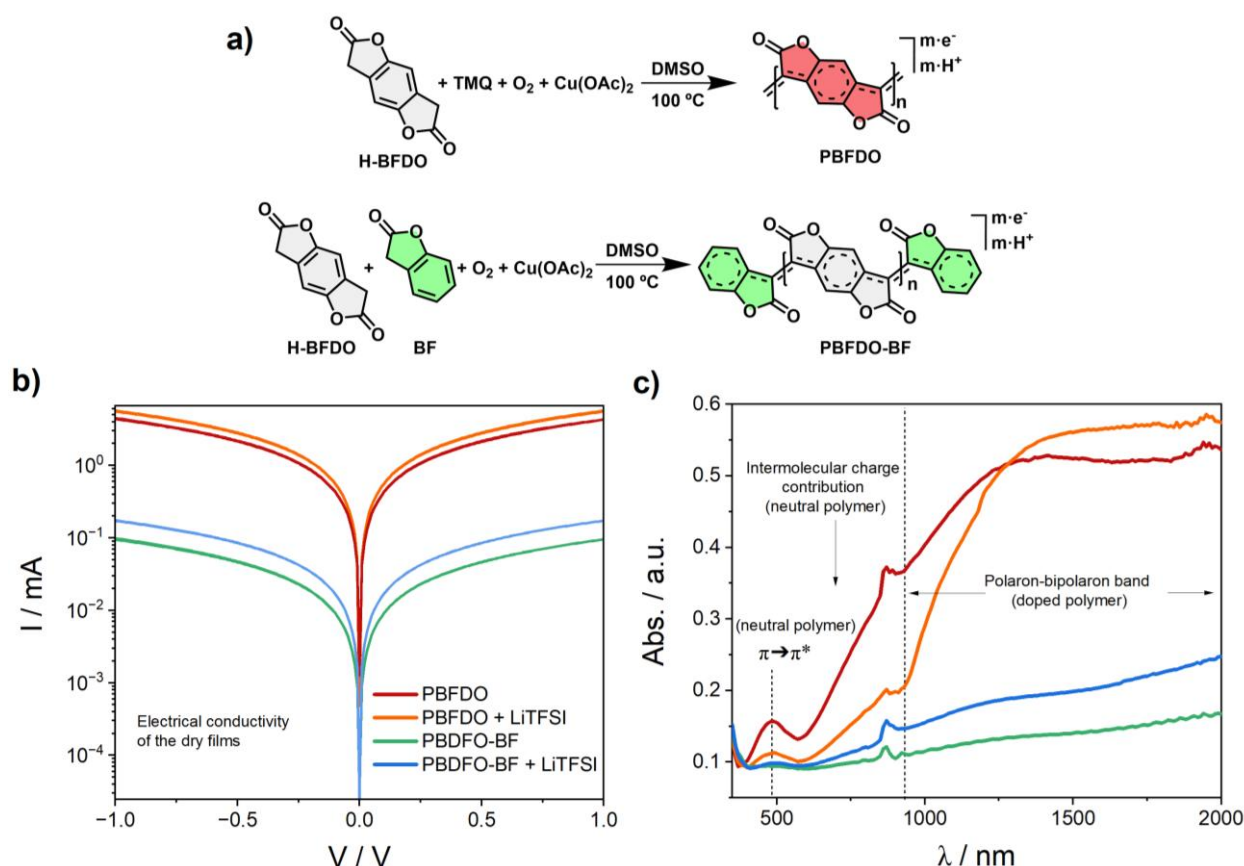


Figure 1. a) Schematic illustration of the oxidative polymerization route for synthesizing PBFDO and end-capped n-PBFDO-BF. b) *I*-*V* characteristics of spin-coated films of PBFDO and PBFDO-BF, with and without 5 wt.% LiTFSI doping. c) UV-vis-NIR absorption spectra of the corresponding polymer films.

As an initial step, we evaluated their behavior in an OECT setup via electrochemical measurements, examining both accumulation and depletion modes, as shown below in **Figure 2a** and **b**. The characterization was carried out by recording first the output OECT characteristic curves, where the drain-source (I_{ds}) current is registered by scanning the drain-source voltage (V_{ds}) at different fixed gate-source voltages (V_{gs}). The gate and drain electrodes shared the same source, which was grounded to ensure a stable reference. Herein, we used 0.1 M NaPF₆ (pH ~ 3) as the electrolyte for characterization, to enable a stable response of the polymer according to our previous work.¹³

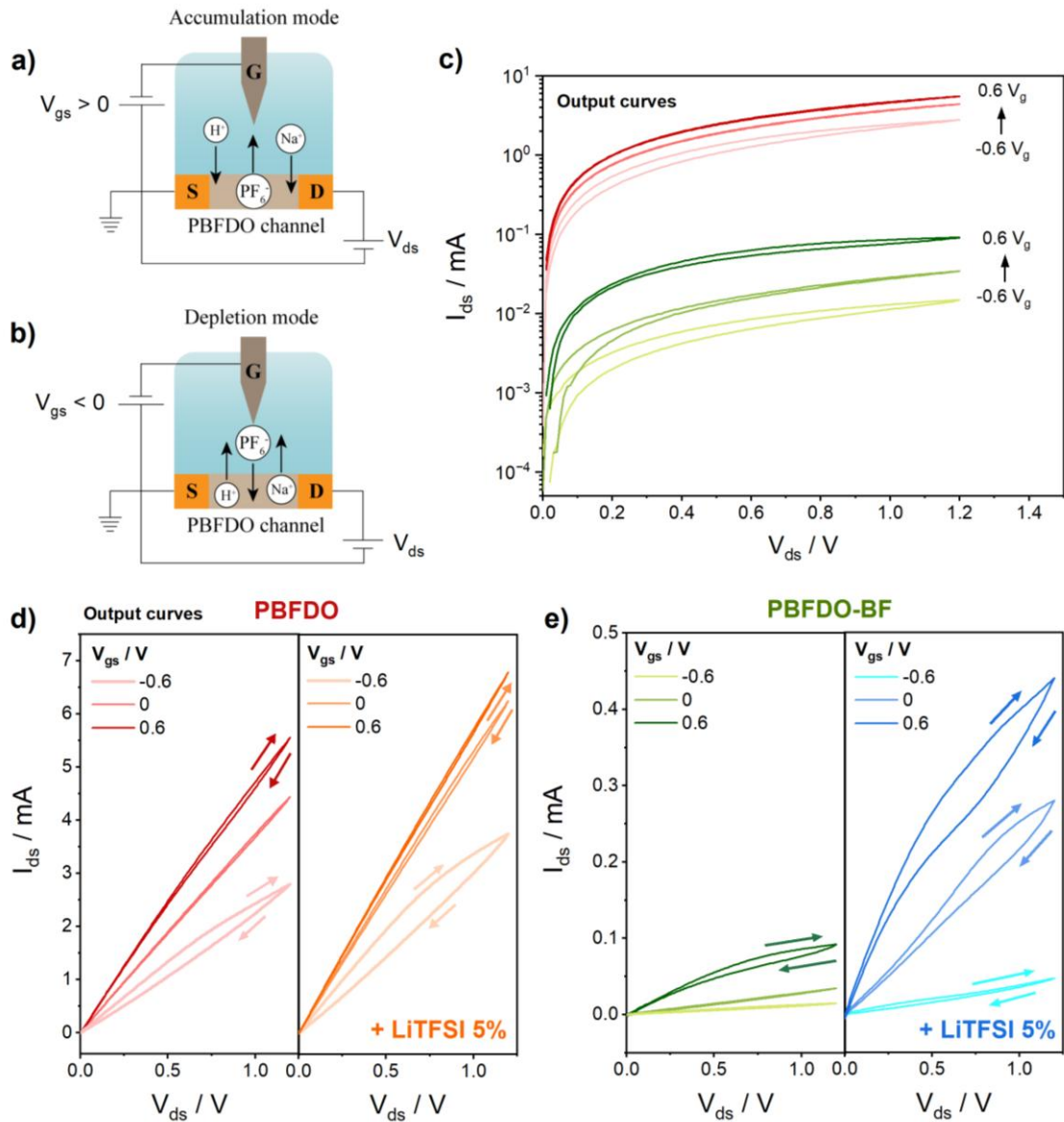


Figure 2. Schematic representation of ion movement a) under positive gate bias and b) under negative gate bias. c) Output characteristic curves of OECTs based on PBFDO and PBFDO-BF polymers operating in accumulation and depletion modes. Comparison of output curves of OECTs fabricated with d) PBFDO and e) PBFDO-BF incorporating 5 wt.% LiTFSI. Electrolyte: 0.1M NaPF₆. Gate electrode: Ag/AgCl wire.

Figure 2c shows the output characteristics of the OECTs based on both PBFDO and PBFDO-BF. The PBFDO devices exhibit a low modulation of I_{ds} by increasing V_{gs} . The output curves display the typical capacitive hysteresis associated with mixed ionic-electronic transport, but the relative change in current after activation remains limited. This behavior suggests that the PBFDO channel is less sensitive to ion-driven doping, due to its already high electronic conductivity. In contrast, the PBFDO-BF devices show a much more pronounced relative dependence on V_{gs} . As positive gate voltages are applied, I_{ds}

increases significantly across the entire V_{ds} range, indicating an efficient electrochemical doping of the polymer. The curves evolve from a low-conductivity regime at $V_{gs} = -0.6$ V to substantially higher current levels at positive biases, which is due to the low intrinsic doping of the PBFDO-BF arising from the synthesis. Applying negative V_{gs} values reversibly reduces I_{ds} in both materials, consistent with channel de-doping. However, the amplitude of de-doping is again more evident in PBFDO-BF, while PBFDO exhibits a comparatively minor decrease in current under the same conditions. These observations confirm that PBFDO-BF undergoes a broader and more effective doping–de-doping window, whereas PBFDO operates in a more electronically dominated regime with limited ionic tunability. The addition of 5 wt.% LiTFSI to PBFDO films (**Figure 2d**) results in only a moderate increase in the current but poor modulation as well, most likely due to the high inherent doping level already present in PBFDO. In contrast, the PBFDO-BF output curves with LiTFSI (**Figure 2e**) display an enhanced modulation by V_{gs} with respect to PBFDO-BF, giving rise to the best gate-triggered doping while maintaining lower currents, which is highly appealing for devices that can be applied in low-energy memory and neuromorphic computing applications. This already demonstrates the effectiveness of the dual strategy based on polymer chain length reduction and LiTFSI-casted predoping during device preparation.

Therefore, we proceeded to investigate the capabilities of the PBFDO-BF + LiTFSI 5 wt.% OECTs for exhibiting memory behavior and synaptic plasticity. **Figure 3a** presents the transfer curves for the PBFDO-BF + LiTFSI 5 wt.% OECTs, which show a sharp increase in I_{ds} at ~ 0.4 V_{gs} , indicating a significant transconductance and fast switching between the OFF (low electrical conductivity) and the ON state (high conductivity). The transfer curves also show significant hysteresis, with lower currents during the forward V_{gs} sweep than in the backward scan back to the initial V_{gs} . This kind of hysteresis in OECTs is related to the capacity of the devices to exhibit memory and synaptic plasticity, making the PBFDO-BF+LiTFSI a promising candidate for neuromorphic computing applications. Devices fabricated with PBFDO-BF+LiTFSI OECT shows the highest relative ON/OFF ratio and hysteresis, while exhibiting low currents, in comparison to the other polymer + additive combination shown in the supplementary material (**Figure SI3** and **SI4**). The PBFDO-BF without LiTFSI doping displays much lower I_{ds} currents but at the expense of a poor V_{gs} modulation. This reflects the low sensitivity to V_{gs} and the reduced doping capacity of the end-capped polymer, also observed in the output curves. The PBFDO-BF requires the salt-casted LiTFSI doping to perform memory applications.

We also investigated the response of the PBFDO-BF+LiTFSI devices to pulse V_{gs} bias, to emulate the type of signals that modulate the synaptic weights in the biological neural networks. **Figure 3b** displays the spike-width-dependent plasticity (SWDP) of the PBFDO-BF+LiTFSI OECTs. The devices show a progressive increase in the pulse current with increasing pulse duration, which also triggers longer relaxation times of the post-pulse current to return to the initial state. The long-term change in conductance after the pulse application, with respect to the initial state, is the effect that can be used as memory or to

simulate synaptic modulation. The devices PBFDO-PB + LiTFSI also show a post-pulse change in conductance modulated by the pulse gate voltage (**Figure 3c**), proving the spike-voltage-dependent plasticity (SVDP) of the devices. The tunable conductance changes with time and amplitude of the pulsating stimuli are widely associated with ion migration and redox-driven doping in conjugated polymers and feature memristive and neuromorphic functionality. The PBFDO-BF without LiTFSI (**Figure SI5**) shows no long-term change in conductance upon V_{gs} pulse application, demonstrating once more the important role of the LiTFSI doping in the synaptic behavior. The PBFDO and PBFDO + LiTFSI OECTs (**Figure SI5** and **SI6**) show high pulse-triggered current increase and long-term change in conductance after the pulse, with no significant changes with the addition of LiTFSI. However, their overall currents are ten times higher than those of the PBFDO-BF+LiTFSI, making them non-competitive in terms of energy efficiency.

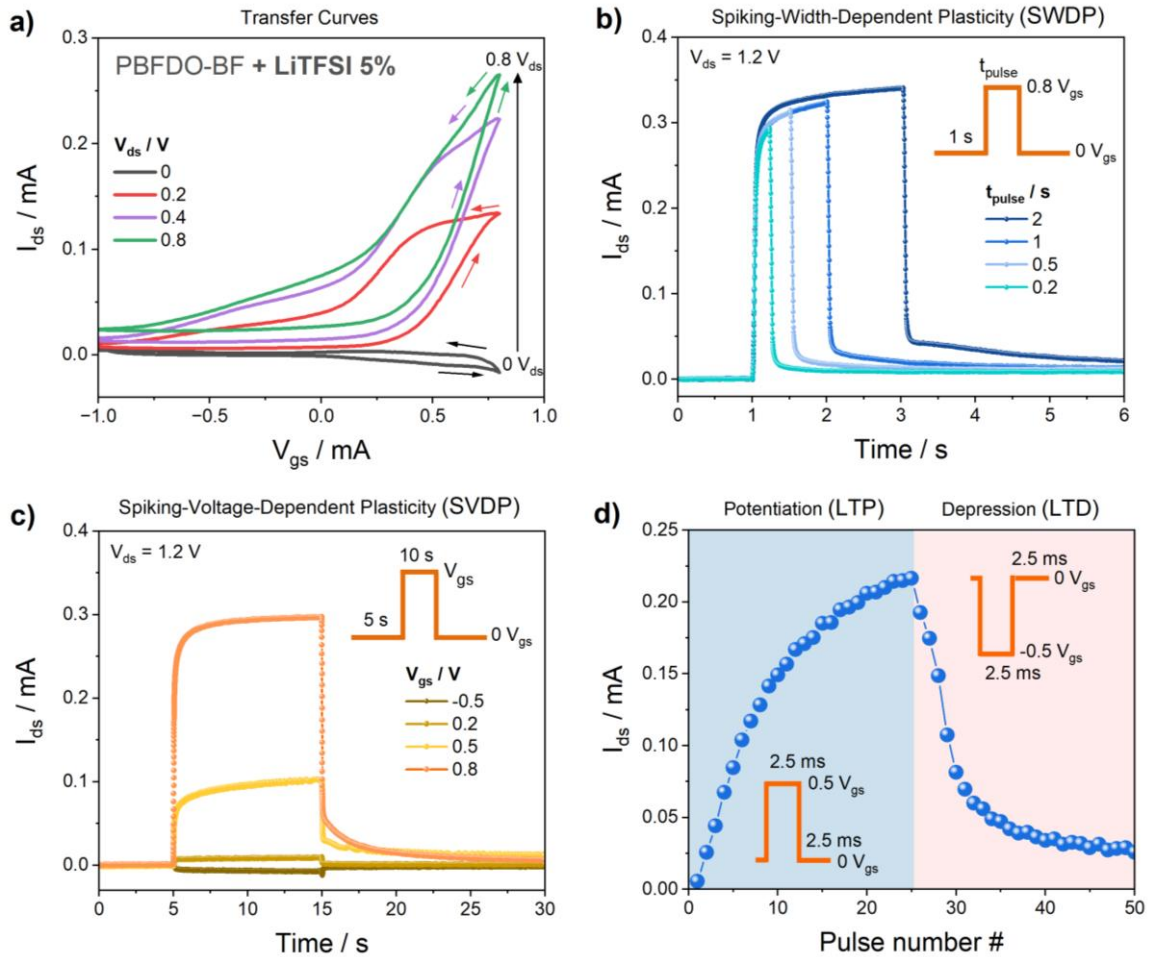


Figure 3. Synaptic response and plasticity of PBFDO-BF+5 wt.% LiTFSI OECTs. a) Transfer characteristics recorded at a scan rate of 30 mV s^{-1} . b) Transient drain-current response under gate-voltage pulses of varying widths (SWDP). Parameters: V_{gs} (pulse) = 0.8 V, V_{gs} (read) = 0 V, $V_{ds} = 1.2 \text{ V}$. c) Transient drain-current response under gate-voltage

pulses of varying amplitudes (SVDP). Parameters: $t_{pulse} = 10$ s , V_{gs} (read) = 0 V, $V_{ds} = 1.2$ V. Devices were pre-deactivated to the OFF state by applying $V_{gs} = -0.8$ V for 20 s. Drain currents are subtracted from the drain currents at $t = 0$. d) Long-term potentiation (LTP) and long-term depression (LTD) cycles, each comprising 25 consecutive set pulses at $V_{gs} = 0.5$ V followed by 25 reset pulses at $V_{gs} = -0.5$ V. V_{gs} (read) = 0 V, $t_{pulse} =$ (a, b) 5 ms, (c, d) 2.5 ms.

To further evaluate the neuromorphic capabilities of the PBFDO-BF + LiTFSI OEECTs, we examined their ability to reproduce the characteristic synaptic functions long-term potentiation (LTP) and long-term depression (LTD). These two processes represent the fundamental mechanisms through which biological synapses strengthen (learning) or weaken (forgetting) their connections (weights) in response to repeated stimuli. In artificial synaptic devices, LTP and LTD typically emerge when ionic migration induces modulated persistent changes in the electronic state of the active material, leading to the non-volatile modulation of channel conductance. **Figure 3d** shows the LTP/LTD curves of the PBFDO-BF + LiTFSI 5 wt.% OEECTs. The PBFDO-BF + LiTFSI OEECT exhibits suitable LTP/LTD cycles with distinguishable states upon the application of 25 doping pulses ($V_{gs} > 0$) to increase the conductance, followed by 25 de-doping pulses ($V_{gs} < 0$). In contrast, OEECTs based on the PBFDO-BF polymer without LiTFSI do not show any measurable potentiation and depression under identical stimulation conditions (**Figure SI7**). This behavior confirms that the limited conductivity, due to a reduced chain length, and restricted ionic penetration, which is essential for synaptic plasticity. PBFDO and PBFDO + LiTFSI 5 wt.% deliver suitable LTP/LTD cycles too (**Figure SI7a and b**), but the currents are ten times higher, as expected from previous characterization.

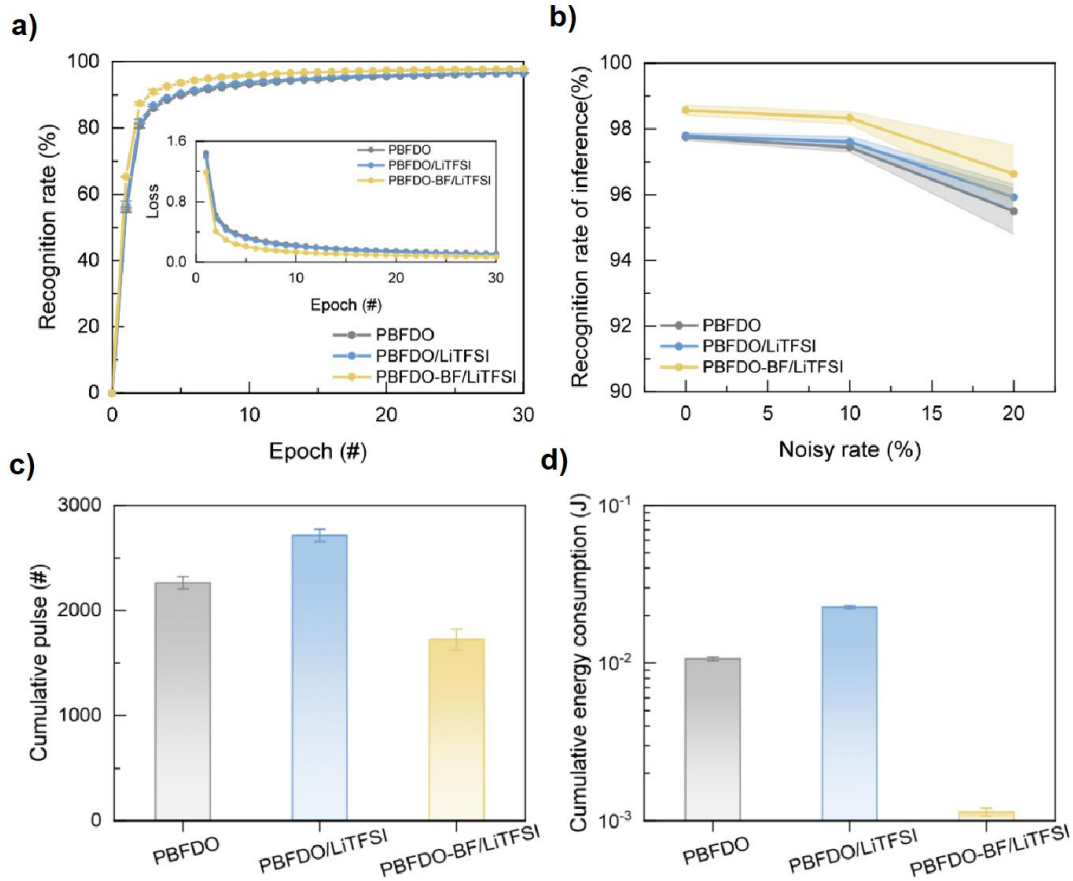


Figure 4. a) Recognition accuracy of PBFDO-series OECTs over 30 training epochs, with insert showing corresponding loss curves. b) Inference accuracy of CNNs based on PBFDO-series OECTs under varying Gaussian noise levels. c) Cumulative programming cost of CNN based on PBFDO-series OECTs, expressed as the number of pulses required to reach $\approx 90\%$ recognition accuracy during CNN training. d) Cumulative energy consumption derived from pulse statistics in (c), with separate evaluation of LTP and LTD contributions to the total energy cost at $\approx 90\%$ recognition accuracy.

In order to validate their applicability, convolutional neural networks (CNNs) were employed to analyze synaptic weights of PBFDO-based OECTs. The neural network (NN) architecture was adapted from previously reported models with appropriate modifications.²² Neuromorphic computing performance was systematically examined for OECTs based on PBFDO, PBFDO + LiTFSI, and PBFDO-BF + LiTFSI. To demonstrate their application potential, recognition accuracy and loss values after 30 training epochs were analyzed (**Figure 4a**). Inference accuracy was further assessed to complement confusion matrix analysis. To probe noise tolerance, Gaussian noise was introduced into the test dataset, enabling direct evaluation of CNN robustness with trained synaptic weights (**Figure 4b**). Finally, energy consumption during CNN training was analyzed using a practical evaluation framework (**Figure 4c**), which provides a more realistic measure of synaptic weight modulation costs compared to metrics derived from a single operating

condition. Overall, this comprehensive analysis highlights the applicability of PBFDO-based OECTs for neuromorphic electronics.

As shown in **Figure 4a**, an MNIST-based CNN model was employed to evaluate the neuromorphic performance of OECTs based on PBFDO, PBFDO + LiTFSI, and PBFDO-BF + LiTFSI. After 30 training epochs, recognition accuracies reached 96.57%, 96.72%, and 97.78% for PBFDO, PBFDO + LiTFSI, and PBFDO-BF + LiTFSI, respectively. Despite the relatively low nonlinearity (NL) of long-term potentiation (LTP) in PBFDO (0.895) and PBFDO + LiTFSI (1.211), their recognition accuracies remain around 96%. In contrast, the PBFDO-BF + LiTFSI device exhibited markedly higher NL in both LTP (3.213) and long-term depression (LTD, 4.105), correlating with its superior recognition accuracy of 97.78%.

In general, pronounced NL is expected to hinder synaptic weight updates during NN training. However, a large dynamic range (DR) can provide a broader conductance window for synaptic weight modulation,²³ which may help compensate for the influence of increased NL during NN training. In particular, the PBFDO-BF + LiTFSI device shows a substantially larger DR (38.99), far exceeding those of PBFDO (2.34) and PBFDO + LiTFSI (2.27). This expanded DR effectively improves the adverse impact of increased NL, thereby enabling superior recognition performance.

Subsequently, the trained CNN with synaptic weights extracted from the PBFDO-series OECTs achieved inference accuracies of 97.74%, 97.79%, and 98.57% on 10,000 handwritten digit images for PBFDO, PBFDO + LiTFSI, and PBFDO-BF + LiTFSI devices, respectively. To further assess noise tolerance, Gaussian noise was introduced into the digit images, as shown in **Figure 4b**. All models maintained robust recognition performance under 10% and 20% noise levels. Notably, the PBFDO-BF + LiTFSI-based CNN sustained a high recognition accuracy of 96.62% even under noisy conditions. This enhanced noise robustness is attributed to side-chain modification of PBFDO, which facilitates ion migration and expands the DR, thereby supporting superior recognition performance.

To reliably evaluate the energy cost of PBFDO-series OECTs in CNN training, **Figure 4c** summarizes the cumulative programming pulses, including both LTP and LTD, required for the models to reach $\cong 90\%$ recognition accuracy. Notably, the PBFDO-BF + LiTFSI OECT required only 1,723 cumulative pulses, markedly fewer than PBFDO (2,265) and PBFDO + LiTFSI (2,715). In addition, the average energy consumption ($E^{\text{avg.}}$) associated with LTP and LTD was quantified using **Equation 1**, providing a consistent framework for evaluating synaptic weight modulation efficiency.

$$E_{LTP,LTD}^{\text{avg.}} = \frac{\sum_{i=0}^n V_D \times I_{DS}(n) \times t}{n} \quad (1)$$

In **Equation 1**, V_D denotes the drain voltage, $I_{DS}(n)$ represents the drain current of the n^{th} pulse, and t is the pulse duration. This framework highlights the energy cost of synaptic

devices during NN training, providing a realistic and application-relevant metric for energy assessment. Accordingly, the E^{avg} of these devices under LTP and LTD conditions is summarized in **Table 1**, showing a pronounced reduction in E^{avg} for side-chain-modified PBFDO-based OECTs. To further evaluate synaptic energy efficiency in CNNs, the analysis was conducted using the models that achieved $\cong 90\%$ recognition accuracy as a baseline. As shown in **Figure 4d**, the cumulative energy consumption of CNNs based on PBFDO, PBFDO + LiTFSI, and PBFDO-BF + LiTFSI OECTs was 0.0106 J, 0.0226 J, and 0.0011 J, respectively. These results indicate that side-chain engineering of conjugated polymers enhances ion migration under an applied electric field, expands the DR of the device, and significantly improves energy efficiency during synaptic weight modulation.

Table 1. Average energy consumption of PBFDO, PBFDO + LiTFSI, and PBFDO-BF + LiTFSI OECTs under LTP and LTD operations.

Pulse State	OECT	E^{avg} ($\mu\text{J}/\text{pulse}$)
LTP	PBFDO	5.18
	PBFDO + LiTFSI	9.51
	PBFDO-BF + LiTFSI	0.94
LTD	PBFDO	3.83
	PBFDO + LiTFSI	6.98
	PBFDO-BF + LiTFSI	0.37

Conclusion

This work demonstrates that the conductivity of PBFDO can be effectively tailored through the synergistic combination of molecular-weight engineering and ionic pre-doping, enabling the fabrication of OECTs with high performance and energy efficiency for neuromorphic applications. Benzofuranone (BF) end-capping reduces polymer chain length and suppresses intrinsic conductivity, but limits ion-mediated conductance modulation. In corporation of 5 wt.% LiTFSI into the end-capped polymer restores efficient ionic control and markedly enhances gate modulation of the low-conductivity PBFDO-BF, yielding the most favorable balance between low-current operation and synaptic functionality. The resulting PBFDO-BF + LiTFS OECTs achieve low-current operation while exhibiting pronounced hysteresis, spike-width- and spike-voltage-dependent plasticity, and well-defined LTP/LTD cycles, confirming their suitability as artificial synapses. At the system level, these improvements translate into superior neuromorphic performance in CNN simulations, with the highest recognition accuracy and the lowest programming energy consumption. Overall, this work establishes molecular-weight control and ionic doping as complementary design strategies for optimizing intrinsically doped n-type polymers toward energy-efficient neuromorphic OECTs.

Experimental Section

Chemicals and materials: Dimethyl sulfoxide (anhydrous, $\geq 99.9\%$, Fischer Scientific), benzofuranone BDF (TCI, $>98\%$), copper(II) acetate (BLDpharm, 98.52%), and 1,3,5-trimethoxybenzene (Sigma-Aldrich, 99.9%) were used for the synthesis and characterization of PBFDO and PBFDO-OH. Tetramethylquinone (TMQ) and lithium bis(trifluoromethanesulfonyl)imide (LiTFSI) were acquired from Sigma Aldrich. NaPF_6 (98%) is acquired from Merck. Interdigitated ITO-prepatterned glass substrates (S161: width \times length: 30 mm \times 50 μm) were acquired from Ossila, and the ITO electrodes were used as the source and drain. All solutions were prepared using ultrapure water ($> 18 \text{ M}\Omega \text{ cm}$) obtained from a Milli-Q system (Merck Millipore, USA).

Synthesis of the PBFDO and PBFDO-BF polymers: The synthesis of the PBFDO and PBFDO-BF polymers was carried out following a procedure analogous to that described by Ke and coworkers (2023).²¹ In the case of PBFDO, the polymer was obtained via copper(II) acetate-catalyzed oxidative polymerization of the monomer H-BFDO in DMSO, with the addition of TMQ as a conductivity-enhancing additive, as reported by Ke et al. The monomer BDF was also synthesized in-house following the article published in 2017 by Singla et al.²⁴ For the synthesis of PBFDO-BF, the monomer H-BFDO was polymerized in the presence of 2 equivalents of benzofuranone (BF), which acted as an end-capping agent, limiting the polymer chain length and resulting in a material with reduced conductivity compared to PBFDO. Both polymerizations were carried out in air and in DMSO (15 mg mL^{-1}) at 100 $^\circ\text{C}$ for 6 h. The resulting polymers were obtained as homogeneous polymer inks purified by dialysis and stored in DMSO. The full conversion of the monomer and the end-capping agent was confirmed by the disappearance of signals in the ^1H -NMR spectra (**Figure S11**).

Fabrication of the OECTs: The PBFDO or PBFDO-BF solution was prepared by diluting the polymer solution coming directly from the reaction (15 mg mL^{-1}) to 10 mg mL^{-1} using DMSO. To prepare the PBFDO + LiTFSI 5% and PBFDO-BF + LiTFSI 5%, a 5% in weight of the LiTFSI salt was dissolved in the polymer solution before deposition. The solution was sonicated at room temperature in an ultrasonic bath for 15 min and stirred with a magnetic stirrer for at least 4 h. Right before deposition, the final polymer solution was filtered with a 45- μm pore size PVDF syringe filter to remove solids. Before deposition, the ITO-patterned substrates were thoroughly washed to clean the surface. First, the substrates were sonicated in deionized (DI) water with detergent for 10 min, followed by rinsing three times with DI water. Second, they were sonicated in acetone and isopropyl alcohol (IPA) for 10 min each. Finally, the substrates were dried using nitrogen flow and treated with a UV-ozone lamp for 15 min to remove any residual organics and improve surface wettability. Polymers were deposited by the spin-coating technique in air atmosphere at 1000 rpm for 1 min. After the spin-coating, the substrates were dried in a vacuum oven at room temperature for at least 5 hours.

Electrochemical measurements: 0.1 M of sodium hexafluorophosphate (NaPF_6) aqueous solution was employed as the electrolyte. An Ag/AgCl wire was employed as the gate

electrode. I-V transfer and output curves of the OECTs were measured using a two-channel Keithley Source Meter controlled by a customized LabVIEW program. The application of V_{gs} pulses during the characterization of the devices towards synaptic plasticity capabilities was conducted using an Agilent 2202B Arbitrary Waveform generator controlled by a customized Python software. For the pulse experiments, I_{ds} was measured using a Metrohm's Autolab PGSTAT204 in coupled with Nova 2.1 software.

UV-Vis-NIR spectra measurements: the transmittance/absorption spectra of all the OECTs were obtained using a UV-VIS-NIR spectrophotometer Lambda 1050+ (Perkin Elmer). Measurements were carried out on freshly-prepared OECT devices in the configuration Glass/ITO/ Polymer.

4-probe electrical conductivity measurements: The electrical conductivity was measured through thin films deposited on glass substrates using the 4-probe method. First, thin films of the polymers were spin-coated on previously washed bare glass substrates using the same conditions described in the fabrication of the OECTs. Next, we deposited Ag fingers by thermal evaporation to be used as electrodes. The evaporation of Ag is carried out under vacuum at 8.5×10^{-6} torr with high control of the evaporation rate. 60 nm Ag is deposited in three steps: i) 0-2 nm thick Ag at 0.1 \AA s^{-1} , 2-10 nm at 0.5 \AA s^{-1} , and 10-60 nm thick Ag: 1 \AA s^{-1}). The electrical conductivity is calculated by measuring the I-V response of the 4-electrode device Ag/PBFDO/Glass by a Metrohm's Autolab PGSTAT204 coupled with Nova 2.1 software. The thicknesses of the polymer films were measured by profilometer.

Convolutional neural network model based on the MNIST database of handwritten digits: The Modified National Institute of Standards and Technology (MNIST) database contains 60,000 handwritten digit images, each with a 28×28 pixel size, of which 10,000 images were used as the test set. The convolutional neural network (CNN) model was constructed with a sequential configuration consisting of one convolutional layer set with 32 filters using 3×3 convolutional kernels, followed by a 2×2 max-pooling layer to preserve the representative image features. These layers were subsequently connected to a fully-connected multilayer perceptron (MLP), which comprised a hidden layer with 128 neurons and an output layer with 10 neurons corresponding to 0 ~ 9 digits. In addition, the long-term potentiation (LTP) and long-term depression (LTD) characteristics extracted from the OECTs were incorporated as synaptic weights to simulate the nonlinear behavior of neuromorphic devices.

Supporting Information

Polymer characterization (H-RMN, 4-probe electrical conductivity, DLS, rheology), OECT electrochemical characterization (additional experiments), and synaptic plasticity study (additional experiments).

Acknowledgements

This work was supported by Grant PID2022-141850OB-C21 (TAROT) funded by MICIU/AEI/10.13039/501100011033 and by ERDF/EU. W.-Y. L. and C.-C. C thank

financial supports from the National Science and Technology Council (NSTC) in Taiwan (112-2223-E-002-008-MY4 and 114-2124-M-027-001). B. I. thanks the Science Committee of the Ministry of Science and Higher Education of the Republic of Kazakhstan for financial support under the project grant No. BR24992852.

References

- (1) Griggs, S.; Marks, A.; Bristow, H.; McCulloch, I. N-Type Organic Semiconducting Polymers: Stability Limitations, Design Considerations and Applications. *J. Mater. Chem. C* **2021**, *9* (26), 8099–8128. <https://doi.org/10.1039/D1TC02048J>.
- (2) Ni, X.; Li, H.; Coropceanu, V.; Brédas, J.-L. Dimensionality-Dependent Electronic Properties of the Highly Conducting n-Type Polymer, Poly(Benzodifurandione). *ACS Mater. Lett.* **2024**, *6* (7), 2569–2576. <https://doi.org/10.1021/acsmaterialslett.4c00624>.
- (3) Kang, S.; Kim, E. C.; Kim, H. W.; Kang, B. Investigation of Poly(Benzodifurandione) for Bioelectronics: High Conductivity, Electrical Stability, and Biocompatibility. *Macromol. Res.* **2025**, *33* (3), 377–383. <https://doi.org/10.1007/s13233-025-00385-8>.
- (4) Ji, H.; Lee, J. G.; Lee, H.; Kim, D.; Cho, K. High-Performance Organic Thermoelectric Materials Based on n-Type Conjugated Polymers via Chemical Isomerization-Induced Charge Transport Modulation. *Mater. Horiz.* **2025**, *12* (21), 9250–9261. <https://doi.org/10.1039/D5MH00991J>.
- (5) Lin, T.; Zeng, F.; Zhong, Z.; He, X.; Sun, Z.; Xu, J. Highly Conductive PBFDO-Based Multifunctional Composite for Electromagnetic Interference Shielding, Thermal Management, and Sensing. *J. Mater. Chem. C* **2025**, *13* (35), 18213–18224. <https://doi.org/10.1039/D5TC01612F>.
- (6) Genene, Z.; Mammo, W.; Wang, E.; Andersson, M. R. Recent Advances in n-Type Polymers for All-Polymer Solar Cells. *Adv. Mater.* **2019**, *31* (22), 1807275. <https://doi.org/10.1002/adma.201807275>.
- (7) Zhang, C.; Huang, H.; Han, S.; Liu, X.; Mo, L.; Zhao, J.; Mo, J.; Che, C. Layer-by-Layer Flexible Organic Thermoelectric Devices Based on PEDOT:PSS and PBFDO. *Energy Mater. Adv.* **2024**, *5*, 0104. <https://doi.org/10.34133/energymatadv.0104>.
- (8) Luo, X.; Yu, J.; Tang, H.; Cai, H.; Xiong, W.; Zhang, K.; Huang, F.; Cao, Y. Self-doped Conjugated Polymers with Electron-deficient Quinone Units for Enhanced Electron Transport in Highly Efficient Organic Solar Cells. *FlexMat* **2024**, *1* (2), 105–115. <https://doi.org/10.1002/flm2.17>.
- (9) Liu, T.; Beket, G.; Li, Q.; Zhang, Q.; Jeong, S. Y.; Yang, C.; Huang, J.; Li, Y.; Stoeckel, M.; Xiong, M.; Van Der Pol, T. P. A.; Bergqvist, J.; Woo, H. Y.; Gao, F.; Fahlman, M.; Österberg, T.; Fabiano, S. A Polymeric Two-in-One Electron Transport Layer and Transparent Electrode for Efficient Indoor All-Organic Solar Cells. *Adv. Sci.* **2024**, *11* (40), 2405676. <https://doi.org/10.1002/advs.202405676>.
- (10) Tang, H.; Liang, Y.; Yang, C.-Y.; Luo, X.; Yu, J.; Zhang, K.; Fabiano, S.; Huang, F. Polyethylene Glycol-Decorated n-Type Conducting Polymers with Improved Ion Accessibility for High-Performance Organic Electrochemical Transistors. *Mater. Horiz.* **2024**, *11* (21), 5419–5428. <https://doi.org/10.1039/D4MH00979G>.
- (11) Xu, J.; Du, K.; Peng, F.; Sun, Z.; Zhong, Z.; Feng, W.; Ying, L. Highly Conductive Polymer Electrodes for Polymer Light-Emitting Diodes. *Npj Flex. Electron.* **2024**, *8* (1), 38. <https://doi.org/10.1038/s41528-024-00324-0>.
- (12) Wu, X.; Tang, H.; Zhou, Z.; Salim, T.; Tang, C. G.; Huang, F.; Leong, W. L. Improved Stability and Performance of an n-Type Depletion Mode Poly(Benzodifurandione) Based Organic Electrochemical Transistor via Electrolyte Selection. *Chem. Mater.* **2024**, *acs.chemmater.4c00867*. <https://doi.org/10.1021/acs.chemmater.4c00867>.
- (13) Sanjuán, I.; Franco, D.; Chen, Q.-G.; Chueh, C.-C.; Lee, W.-Y.; Guerrero, A. Proton Migration-Modulated n-Doped Poly(Benzodifurandione) Organic Electrochemical Transistors Used for Neuromorphic Computing Applications. *ACS Energy Lett.* **2025**,

- 10 (11), 5209–5217. <https://doi.org/10.1021/acsenergylett.5c02076>.
- (14) Zhao, C.; Yang, J.; Ma, W. Transient Response and Ionic Dynamics in Organic Electrochemical Transistors. *Nano-Micro Lett.* **2024**, *16* (1), 233. <https://doi.org/10.1007/s40820-024-01452-y>.
 - (15) Sun, S.; You, Z.; Ji, Y.; Li, Y.; Feng, Y.; Liu, S.; Cao, J.; Liu, Y.; Yu, Z.; Wu, T. Application and Challenges of Organic Electrochemical Transistors in Neuromorphic Computing: Bionic Synapse and Multi-Mode Integration. *J. Mater. Chem. C* **2025**, *13* (37), 19125–19148. <https://doi.org/10.1039/D5TC02381E>.
 - (16) Bisquert, J.; Ilyassov, B.; Tessler, N. Switching Response in Organic Electrochemical Transistors by Ionic Diffusion and Electronic Transport. *Adv. Sci.* **2024**, *11* (36), 2404182. <https://doi.org/10.1002/advs.202404182>.
 - (17) Tang, H.; Liang, Y.; Liu, C.; Hu, Z.; Deng, Y.; Guo, H.; Yu, Z.; Song, A.; Zhao, H.; Zhao, D.; Zhang, Y.; Guo, X.; Pei, J.; Ma, Y.; Cao, Y.; Huang, F. A Solution-Processed n-Type Conducting Polymer with Ultrahigh Conductivity. *Nature* **2022**, *611* (7935), 271–277. <https://doi.org/10.1038/s41586-022-05295-8>.
 - (18) Li, N.; Sheng, H.; Sun, Y.; Wang, J. Spectroscopic Study on Size-Dependent Optoelectronics of N-Type Ultra-High Conductive Polymer PBFDO. *Spectrochim. Acta. A. Mol. Biomol. Spectrosc.* **2023**, *298*, 122744. <https://doi.org/10.1016/j.saa.2023.122744>.
 - (19) Zhao, C.; Yang, J.; Ma, W. Transient Response and Ionic Dynamics in Organic Electrochemical Transistors. *Nano-Micro Lett.* **2024**, *16* (1), 233. <https://doi.org/10.1007/s40820-024-01452-y>.
 - (20) Ohayon, D.; Flagg, L. Q.; Giugni, A.; Wustoni, S.; Li, R.; Hidalgo Castillo, T. C.; Emwas, A.-H.; Sheelamanthula, R.; McCulloch, I.; Richter, L. J.; Inal, S. Salts as Additives: A Route to Improve Performance and Stability of n-Type Organic Electrochemical Transistors. *ACS Mater. Au* **2023**, *3* (3), 242–254. <https://doi.org/10.1021/acsmaterialsau.2c00072>.
 - (21) Ke, Z.; Abtahi, A.; Hwang, J.; Chen, K.; Chaudhary, J.; Song, I.; Perera, K.; You, L.; Baustert, K. N.; Graham, K. R.; Mei, J. Highly Conductive and Solution-Processable n-Doped Transparent Organic Conductor. *J. Am. Chem. Soc.* **2023**, *145* (6), 3706–3715. <https://doi.org/10.1021/jacs.2c13051>.
 - (22) Liu, C.-J.; Hsiao, S.-W.; Chen, Q.-G.; Hong, Q.-A.; Lin, Y.-T.; Chueh, C.-C.; Ng, C.-T.; Chang, T.-T.; Kim, S. H.; Chiu, Y.-C.; Lee, W.-Y. Polarizable Thiol–Ene Cross-Linked Nitrile Dielectrics for Stretchable Low-Voltage Neuromorphic Transistors with Acoustic Classification. *ACS Appl. Mater. Interfaces* **2026**, acsami.5c18342. <https://doi.org/10.1021/acscami.5c18342>.
 - (23) Kim, S.; Choi, B.; Lim, M.; Yoon, J.; Lee, J.; Kim, H.-D.; Choi, S.-J. Pattern Recognition Using Carbon Nanotube Synaptic Transistors with an Adjustable Weight Update Protocol. *ACS Nano* **2017**, *11* (3), 2814–2822. <https://doi.org/10.1021/acsnano.6b07894>.
 - (24) Singla, P.; Van Steerteghem, N.; Kaur, N.; Ashar, A. Z.; Kaur, P.; Clays, K.; Narayan, K. S.; Singh, K. Multifunctional Geometrical Isomers of Ferrocene-Benzo[1,2-b:4,5-B']Difuran-2,6-(3H,7H)-Dione Adducts: Second-Order Nonlinear Optical Behaviour and Charge Transport in Thin Film OFET Devices. *J. Mater. Chem. C* **2017**, *5* (3), 697–708. <https://doi.org/10.1039/C6TC03876J>.